Journal of Power Sources 196 (2011) 2380–2386

Contents lists available at ScienceDirect

Journal of Power Sources

journal homepage: www.elsevier.com/locate/jpowsour

High energy density capacitor using coal tar pitch derived nanoporous carbon/MnO_2 electrodes in aqueous electrolytes

Timothy Tomko[a], Ramakrishnan Rajagopalan[b,*], Michael Lanagan[b], Henry C. Foley[c]

[a] Energy and Mineral Engineering, University Park, PA 16802, USA
[b] Materials Research Institute, University Park, PA 16802, USA
[c] Department of Chemical Engineering, University Park, PA 16802, USA

ARTICLE INFO

Article history:
Received 27 August 2010
Accepted 1 October 2010
Available online 8 October 2010

Keywords:
Coal tar pitch
Manganese dioxide
High energy density
Activated carbon
Asymmetric capacitor

ABSTRACT

Asymmetric aqueous electrochemical capacitors with energy densities as high as 22 Wh kg^{-1}, power densities of 11 kW kg^{-1} and a cell voltage of 2 V were fabricated using cost effective, high surface carbon derived from coal tar pitch and manganese dioxide. The narrow pore size distribution of the activated carbon (mean pore size ~0.8 nm) resulted in strong electroadsorption of protons making them suitable for use as negative electrodes. Amorphous manganese dioxide anodes were synthesized by chemical precipitation method with high specific capacitance (300 F g^{-1}) in aqueous electrolytes containing bivalent cations. The fabricated capacitors demonstrated excellent cyclability with no signs of capacitance fading even after 1000 cycles.

1. Introduction

The concept of integrating a redox or battery type electrode and a double layer electrode has been widely used to develop high energy density hybrid capacitors in both aqueous and non-aqueous electrolytes [1–4]. In particular, cost effective redox active metal oxides, such as manganese dioxide (MnO_2) electrodes, have been combined with activated carbon (AC) electrodes with a narrow pore size distribution to produce aqueous electrochemical capacitors with cell voltages as high as 2.0 V and energy densities greater than 15 Wh kg^{-1} [5–8].

Manganese dioxide has been shown to have specific capacitances in the order of 300–600 F g^{-1}. Very high specific capacitances are usually demonstrated when these metal oxides are deposited as thin films on high surface area conductive supports such as carbon nanotubes [9–11]. Bulk synthesis of manganese dioxide powder with a high surface area and a specific capacitance approaching 300 F g^{-1} has also been synthesized [12]. It has also been shown that with the variation of cations, monovalent or bivalent, in the electrolyte, the specific capacitance of MnO_2 can be significantly increased. Asymmetric capacitors with excellent cyclability greater than 1000 cycles were demonstrated using calcium nitrate as the aqueous electrolyte [5,6].

Activated carbon with mean pore sizes less than 1.0 nm has shown a strong affinity for the electroadsorption of protons. This phenomenon manifests itself as a capacitive response between 0 and −1.0 V vs. Ag/AgCl [13–17]. By carefully accounting for the charge stored in both of the electrodes, it is possible to extend the cell voltage for the asymmetric devices to almost 2.0 V without violating the thermodynamic limits imposed by electrolysis of water. From a practical standpoint, it is imperative to design synthetic routes to make these high surface area carbons from low cost precursors. Coal tar pitch (CTP) is one promising low cost carbon precursor. However, when CTP is pyrolyzed, it leads to polycrystalline graphite, which is non-porous and therefore not useful for ultracapacitor applications. Moreover, most pitches soften at temperatures between 300 and 500 °C and form dense mesophases making them difficult to activate. To create porosity in CTP, one has to consider the precursor – how it will be pretreated and how the carbon derived from it will be post treated. Most researchers have used alkali-catalyzed oxidation for the development of extra porosity in low porosity carbons [18–20]. Pitch derived carbonaceous materials activated using KOH can have apparent N_2 BET surface areas that approach 3200 m^2 g^{-1} with specific capacitance values as high as 320 F g^{-1} in aqueous sulfuric acid [21–23]. But chemical activation requires an exhaustive washing procedure to remove the alkali making the process more cost intensive and the purity of the carbon is always a problem. KOH activation also leads to carbon with a very low bulk density, an important parameter for determining the volumetric capacitance of the carbon. Alternatively, physical activation using steam or CO_2 avoids contamination

* Corresponding author. 270 MRL Bldg., University Park, PA 16802, USA. Tel.: +1 814 863 1880; fax: +1 814 863 8561.
E-mail address: rur12@psu.edu (R. Rajagopalan).

0378-7753/$ – see front matter © 2010 Elsevier B.V. All rights reserved.
doi:10.1016/j.jpowsour.2010.10.004

since it is a simple burn-off process [24,25]. However, it is usually ineffective at creating porosity in pitch derived carbons [18].

In this investigation, coal tar pitch has been modified to yield a highly disordered carbon which upon physical activation, using CO_2, results in a high surface area carbon with a narrow pore size distribution. The use of these carbons as electrodes in high energy density aqueous asymmetric capacitors has been demonstrated.

2. Experimental

2.1. Synthesis of electrode materials

2.1.1. Activated carbon from coal tar pitch

Koppers Inc. supplied coal tar pitch (CTP) that contains 5.2 wt% quinoline insolubles. A sample of 5 g of CTP was dissolved in 50 mL of tetrahydrofuran (THF) and allowed to stir for 2 h. The dissolved mixture was then filtered using vacuum filtration; the filtrate (THF soluble) was collected (yield ~70%). The THF soluble fraction was then mixed with H_2SO_4 (1:2 by wt.) and stirred overnight. The resultant viscous solution (modified CTP) was placed in a tube furnace under flowing argon and heated to 160 °C in 1 h. The sample remained at this temperature for 4 h, and then was increased to 800 °C in 4 h and maintained at 800 °C for an additional 8 h.

The pyrolyzed sample was then heated under argon atmosphere to 900 °C in 1 h and held at 900 °C for another hour, whereupon it was activated under flowing CO_2 to yield an activated carbon with 65 wt% burn-off. After activation, the sample was cooled to room temperature under flowing argon.

2.1.2. Synthesis of manganese dioxide powders

The synthesis of high surface area manganese dioxide was adapted from the procedure described by Subramanian et al. [26]. 0.5 g of potassium permanganate ($KMnO_4$) was dissolved in 10 mL of water in a small beaker. 50 mg of Triton-X 100 surfactant, 20 mL of hexane, and 5 mL of methanol were mixed in a separate beaker and the two solutions were combined together by slowly adding dropwise the surfactant mixture to the aqueous $KMnO_4$. The resultant mixture was stirred and ultrasonicated for 10 min and a color change from purple to brown was observed. The solution was filtered and rinsed thoroughly several times to ensure no surfactant remained in the sample. The solid residue was then dried at 100 °C to constant weight and the yield was 76%.

2.2. Characterization of activated carbon and manganese dioxide

The pore size distribution of the carbon was calculated using methyl chloride adsorption. The pore sizes were determined using H–K model described elsewhere [27]. N_2 adsorption and desorption isotherms were collected for AC by measuring the N_2 uptake of the AC at 77 K. The apparent N_2 BET surface areas were also measured using standard methodology from adsorption isotherms. Approximately, 0.2 g of sample was used for the experiment and the samples were baked at 100 °C under dynamic vacuum overnight before the experiment. The morphology and the particle size of the electrode materials were studied using a Hitachi S-3000 H SEM. XPS measurements (Kratos Analytical Axis ultra Instrument, Chestnut Ridge, NY)) were done in order to study the oxidation state of manganese in MnO_2. Powder X-ray diffraction technique was used to determine the composition of the synthesized MnO_2 using a Scintag X2 powder Diffractometer.

2.3. Electrochemical characterization

2.3.1. Three-electrode electrochemical testing

The AC electrode was prepared by combining 0.085 g AC, 0.01 g Teflon binder and 0.005 g of acetylene black. The resultant powder was then dispersed in 1 mL of THF and the solution was ultrasonicated for 20 min. 2 mg of the resultant slurry was applied to 1 cm^2 of carbon fiber mat (supplied by Technical fibres Inc.) and blown dry to constant weight. Similarly, 0.07 g of manganese dioxide, 0.01 g of Teflon binder, and 0.02 g of acetylene black were used to create the manganese dioxide slurry and was applied onto the carbon fiber mat.

All electrochemical measurements were done using a 263A Potentiostat/Galvanostat. The active electrode materials were tested individually as the working electrodes using a platinum wire as a counter electrode and Ag/AgCl as a reference electrode in various aqueous salt solutions (2 M KCl, $MgCl_2$, and $CaCl_2$ respectively). The pH of the aqueous electrolytes were adjusted in the range of 5–8 and the cyclic voltammograms were measured at a scan rate of 2 mV s^{-1} using a scan range of 0.3 to −1 V for AC and 0 to 1 V for manganese oxide vs. Ag/AgCl, respectively.

2.3.2. Two-electrode ultracapacitor

AC and MnO_2 slurries were made similar to the three-electrode experiments. The mass of MnO_2 electrode was held constant at 2 mg for all the experiments while the mass of the AC electrode varied from 2 to 4 mg depending upon the electrolyte system. Prior to assembly of the cell, the AC and MnO_2 electrodes, as well as a Celgard 3501 membrane, were soaked in the aqueous electrolyte, under vacuum, for 30 min. Tantalum foils were used as the current collectors for both electrodes. The two electrode capacitor was assembled together such that the AC was used as the negative electrode and the reference electrode, while MnO_2 was used as the positive electrode. The cell was then submerged in aqueous electrolyte and tested using cyclic voltammetry, electrochemical impedance spectroscopy and constant current charge/discharge cycling. Cyclic voltammetry was done using a scan range of 0–2.0 V at a scan rate of 10 mV s^{-1} for 100 cycles. The EIS measurements were done using a model 5210 Lock-in amplifier coupled with 263A Potentiostat/Galvanostat. An ac perturbation of 10 mV was applied at open circuit voltage conditions. The frequency of the ac perturbation was varied from 10^5 to 10^{-3} Hz. The equivalent series resistance (ESR) of the cell was computed using the impedance data measured at 100 Hz. The obtained data was fitted to an equivalent circuit model using ZView software. Galvanostatic charge/discharge cycling was done by applying a load current density ranging from 200 mA g^{-1} to 6 A g^{-1} and the charge/discharge measurements were recorded up to 1000 cycles. Specific capacitance, energy density and power densities were computed from the discharge curves.

3. Results

3.1. Synthesis and characterization of electrode materials

Fig. 1a and b show the methyl chloride pore size distribution of the carbons derived from coal tar pitch. Carbon derived from pyrolysis of as received CTP at 900 °C has a very low N_2 BET surface area (0.6 m^2 g^{-1}) and no measurable porosity. Upon activation using CO_2 at 900 °C, the surface area increases slightly to 150 m^2 g^{-1}. However, the activated carbon does not have any measurable nanoporosity (as received CTP). When the pitch was modified using H_2SO_4 and pyrolyzed, it resulted in a modest nanoporous carbon with narrow pore size distribution centered at 0.5 nm (pyrolyzed modified pitch). Upon CO_2 activation, the sample (AC) had a surface area of 1700 m^2 g^{-1} with broader pore size distribution than the modified CTP and a mean pore size of 0.8 nm. The nanopore volume significantly increased to 0.7–0.8 cc g^{-1} as shown in Fig. 1b. Our results were further confirmed using N_2 BET surface area measurements, which show a type I isotherm

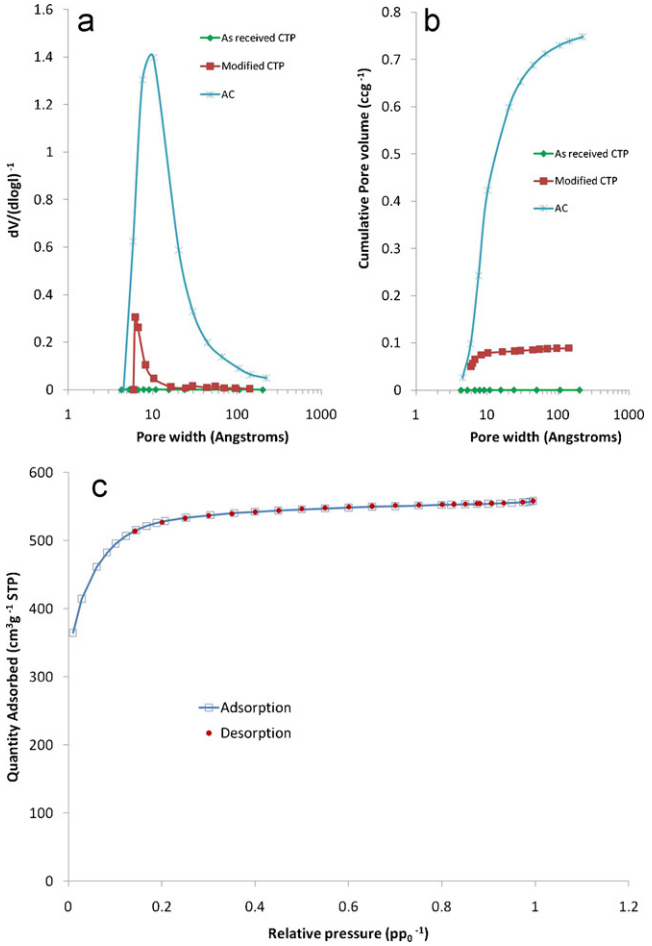

Fig. 1. (a) Pore size distribution and (b) Cumulative pore volume of carbons derived from coal tar pitch measured using methyl chloride adsorption unit; (c) N_2 adsorption and desorption isotherms of activated coal tar pitch (AC).

without a hysterisis indicating a completely microporous carbon (Fig. 1c).

Fig. 2 shows the SEM micrographs of AC and MnO_2, respectively. AC had a faceted morphology and large average particle size ~20–30 μm (Fig. 2a). The MnO_2 powders had an agglomerated morphology with average grain size in the order of ~200 nm with a N_2 BET surface area of 130 $m^2\,g^{-1}$ (Fig. 2b).

XRD of the synthesized MnO_2 powders indicated that the sample was amorphous as seen by the broad amorphous peak between 30° and 40° (Fig. 3a). To determine the oxidation state of Mn in its oxide forms, the multiplet splitting of Mn 3s peaks in the XPS spectrum has been used in the literature [28–30]. The oxidation state is determined by measuring the difference in the binding energy of the two split peaks (ΔE). As shown in Fig. 3b, the ΔE value of the as prepared MnO_2 sample was 4.98 eV. This value lies between 4.7 and 5.3 eV corresponding to Mn^{4+} and Mn^{3+} respectively. Hence, the mean oxidation state of Mn in the synthesized sample was about 3.5.

3.2. Three-electrode measurements

The electrode materials were tested in different aqueous electrolytes at a scan rate of 2 mV s^{-1}. The specific capacitances of the individual electrodes from the three-electrode experiments were measured as follows:

$$C = \frac{Q_a + |Q_c|}{2V\upsilon m} \quad (1)$$

where Q_a and Q_c are the anodic and cathodic charges respectively in Coulombs; V is the scan range in Volts; υ is the scan rate in V s^{-1}; m is the mass of the active material in g.

The specific capacitance of AC measured in the scan range of 0.3 to −1.0 V vs. Ag/AgCl was 75 F g^{-1} while the capacitance of MnO_2 was dependent on the nature of the electrolyte. The specific capacitance of MnO_2 ranged from 160 F g^{-1} in aqueous KCl to almost 300 F g^{-1} in aqueous $MgCl_2$ electrolyte. In spite of the high specific capacitance in $MgCl_2$, the cyclable voltage range of MnO_2 was limited to a scan range of 0.3–1.0 V vs. Ag/AgCl as shown in Fig. 4a due to the steep increase in current below 0.3 V. On the other hand, KCl and $CaCl_2$ provided a larger stable scan range (0–1.0 V vs. Ag/AgCl). The specific capacitance was also sensitive to the pH of the electrolyte. It was seen that the optimum pH range for the electrolytes was 6–7 as shown in Fig. 4b.

3.3. Two electrode measurements

Based on the specific capacitance and stable voltage ranges of the individual electrodes, asymmetric capacitors were constructed using AC and MnO_2 in three different electrolytes. The mass ratio of the two electrodes was adjusted in the following manner to ensure the charge on each electrode was equal:

$$Q = C_{AC}\,V_{AC}\,m_{AC} = C_{MnO_2}\,V_{MnO_2}\,m_{MnO_2} \quad (2)$$

where Q is the total charge on each electrode in Coulombs; C_{AC} and C_{MnO_2} is the specific capacitance of the AC and MnO_2 electrodes in

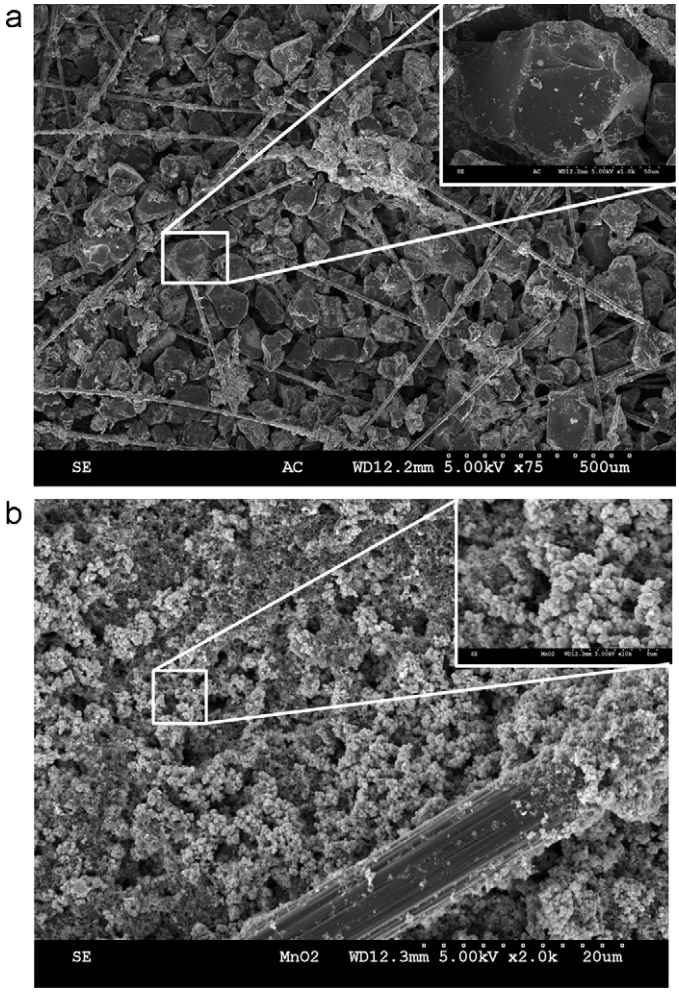

Fig. 2. SEM micrographs of (a) AC and (b) MnO_2.

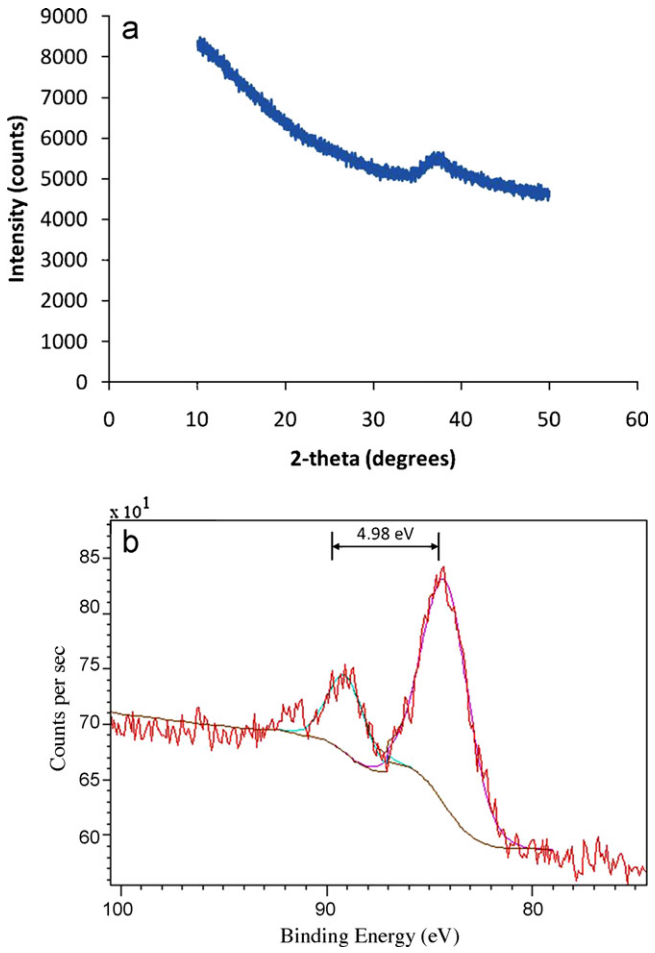

Fig. 3. (a) XRD of synthesized MnO_2; (b) Mn 3s XPS spectrum of MnO_2.

$F g^{-1}$; V_{AC} and V_{MnO_2} is the scan range of the AC and MnO_2 electrodes in Volts; m_{AC} and m_{MnO_2} is the mass of active material on the AC and MnO_2 electrodes in grams

Fig. 5 shows the overlay of cyclic voltammograms of asymmetric capacitor in different electrolytes. The voltammograms of the two electrode capacitors were measured using a scan range from 0 V to a maximum of 2 V at 10 mV s^{-1} for 100 cycles.

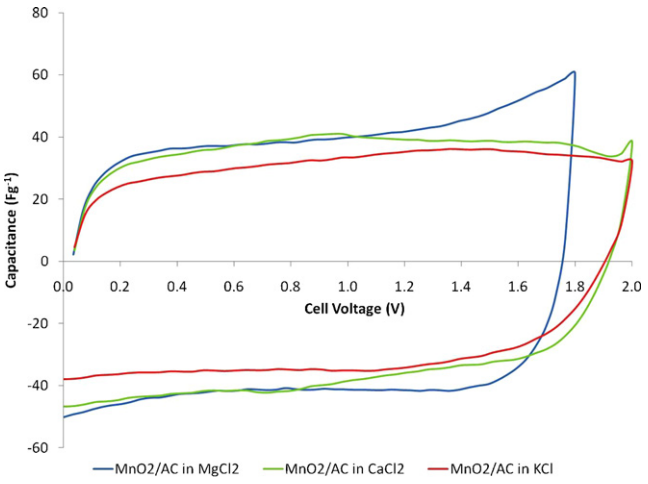

Fig. 5. Specific capacitance of asymmetric capacitors measured using cyclic voltammetry in three different electrolytes measured at a scan rate of 10 mV s^{-1} after 100 cycles.

Table 1
Parameters used to fabricate asymmetric capacitors with AC and MnO_2 in three different electrolytes.

Electrolyte	C_{AC} ($F g^{-1}$)	C_{MnO_2} ($F g^{-1}$)	m_{AC}/m_{MnO_2}	Cell voltage (V)
$MgCl_2$	75	307	1.00:1	1.8
$CaCl_2$	75	254	1.60:1	2.0
KCl	75	161	1.36:1	2.0

The specific capacitance of the cell was calculated as shown in Eq. (3).

$$C = \frac{I}{\upsilon m} \tag{3}$$

where I is the anodic or cathodic current in Amperes; υ is the scan rate in V s^{-1}; m is the total active mass of both the electrodes in grams.

Since the energy density of the asymmetric capacitor was limited primarily by the mass of the AC electrode in aqueous electrolyte systems [31], the asymmetric capacitor was fabricated such that amount of AC on the negative electrode was kept to a minimum. Table 1 shows the ratio of AC: MnO_2.

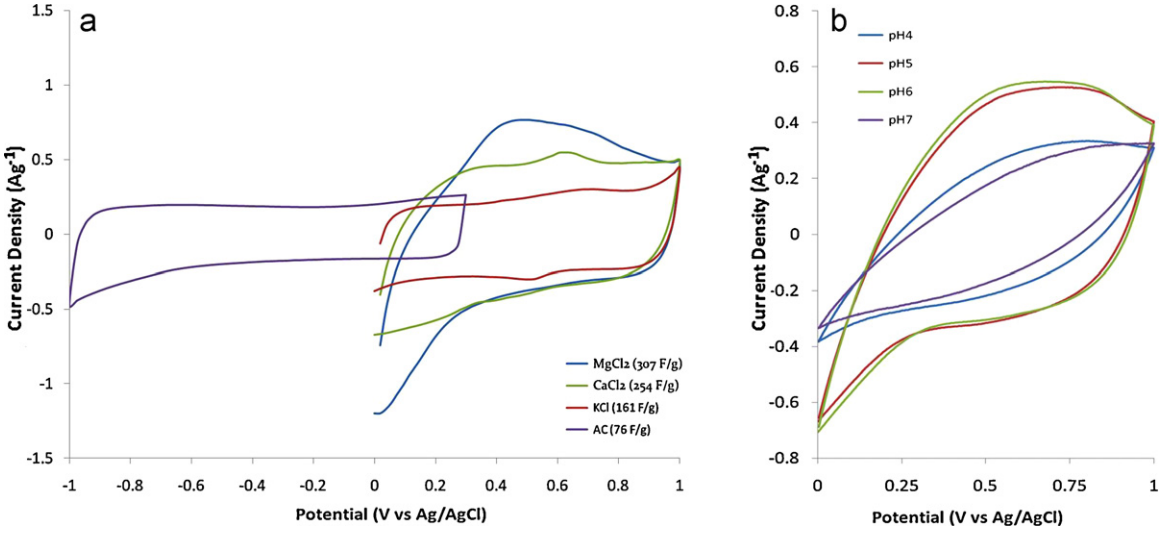

Fig. 4. Three-electrode cyclic voltammetry measurements after 100 cycles at a scan rate of 2 mV s^{-1} of (a) AC in 2 M $CaCl_2$ and MnO_2 in 2 M $MgCl_2$, $CaCl_2$ and KCl after 100 cycles; (b) Effect of variation of pH of 2 M $MgCl_2$ on the cyclic voltammagram of MnO_2.

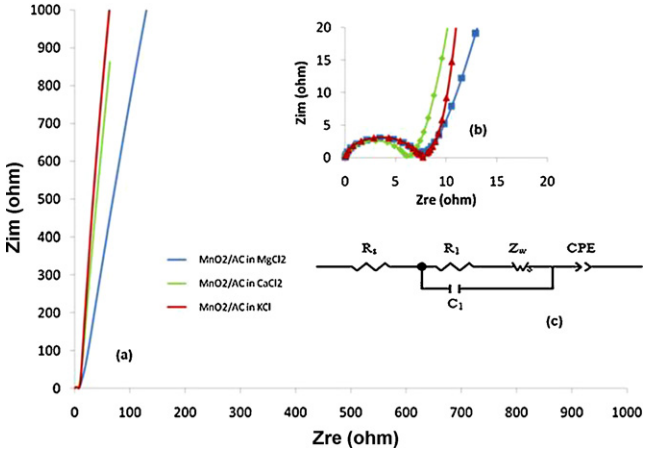

Fig. 6. (a) Nyquist plot of asymmetric capacitors measured in three different electrolytes, (b) Nyquist plots fitted using an equivalent circuit model and (c) Equivalent circuit model.

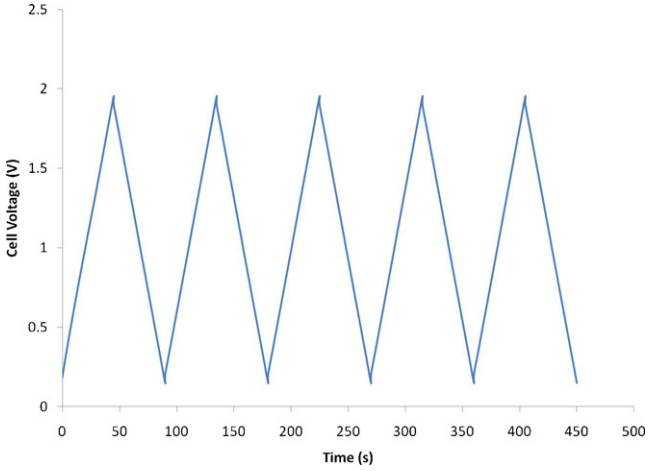

Fig. 7. Constant current charge/discharge profile of asymmetric capacitor made using AC and MnO_2 in aqueous $CaCl_2$ measured at a specific load current density of 1.5 A g^{-1} for 1000 cycles.

Based on Eq. (2), this would result in a cell voltage of 2 V for $CaCl_2$ and KCl respectively and 1.8 V for $MgCl_2$. The cell capacitance in aqueous KCl was 35 F g^{-1} while the capacitance in aqueous $CaCl_2$ and $MgCl_2$ was 40 and 45 F g^{-1}, respectively.

EIS measurements were done to calculate the ESR of the asymmetric capacitors (Fig. 6). Aqueous KCl and $MgCl_2$ systems had ESR of 8 Ω while the $CaCl_2$ system was slightly lower (6.5 Ω). The Nyquist plots for all the three systems showed a semicircle at high frequencies followed by a steep linear increase at low frequencies. An equivalent circuit was fitted to the impedence spectra as shown in Fig. 6.

Five different contributions namely R_s, R_1, Z_w, C_1 and CPE were computed. R_s corresponds to sum total of all the series resistance contributions that include contact resistance with the current collector, electronic resistance of electrode material and solution resistance of the electrolytes. R_1 corresponds to the contributions at the grain boundary of the electrode materials such as charge transfer resistance in MnO_2 and grain boundary resistance in AC. Z_w corresponds to the Warburg contribution to the impedence due to the bulk diffusion of the ions to the electrode/electrolyte interface, C_1 is the contribution to the capacitance at each grain boundary layer and CPE refers to a constant phase element that represents collectively the double layer/pseudocapacitive contribution at each electrode of the capacitor. The CPE was used to account for dispersion in the capacitive behavior at the electrodes due to variation in pore size distribution of AC and pseudocapacitive behavior of MnO_2. The two parameters T and P for the CPE was obtained from the fit and its contribution to the overall impedence are as follows:

$$Z = \frac{1}{T(j\omega)^P} \tag{4}$$

where Z is the impedence in ohm; T and P are the CPE parameters, respectively; ω is the angular frequency in rad s^{-1}.

An ideal capacitor would have a value close to $P = 1$. As shown in Table 2, the value of P for all the systems was 0.93–0.96 indicating a highly capacitive behavior.

Table 2
Fitted parameters of equivalent circuit model.

System	R_1 (Ω)	R_2 (Ω)	Z_w (Ω)	C_1 (μF)	CPE	
					T	P
KCl	0.59	6.20	0.02	11.00	0.10	0.96
$CaCl_2$	1.05	4.85	0.05	10.00	0.16	0.96
$MgCl_2$	1.08	6.00	0.02	8.73	0.08	0.93

Constant current charge/discharge measurements were done at various load current densities ranging from 200 mA g^{-1} to 6 A g^{-1}. The charge discharge curves vary linearly with potential indicating capacitive response (Fig. 7).

The coulombic efficiency given by the ratio of time of charge and discharge was greater than 99% for all the systems and for 1000 cycles. The specific capacitance was calculated from the discharge curve as follows:

$$C = \frac{i\,\Delta t}{\Delta V} \tag{5}$$

where i is the specific current density in A g^{-1}; Δt is the discharge time in seconds; ΔV is the potential drop during discharge in Volts

Fig. 8 shows the cycle life performance of the asymmetric capacitors. The cell capacitance was measured from the charge/discharge curves and showed no degradation over the entire 1000 cycles. The cell capacitance increased in the order $MgCl_2$ > $CaCl_2$ > KCl system.

Energy density and power density of the capacitors were measured using the cell capacitance, cell voltage and load current from the galvanostatic charge/discharge measurements as follows:

$$E = \frac{1}{2}C\Delta V^2 \tag{6}$$

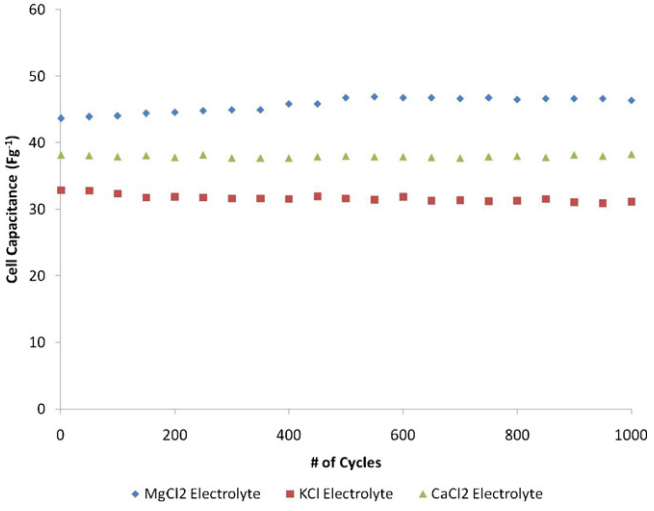

Fig. 8. Cycling stability of asymmetric capacitors studied using constant current charge/discharge measurements with three different electrolytes at a load current density of 1.5 A g^{-1} for 1000 cycles.

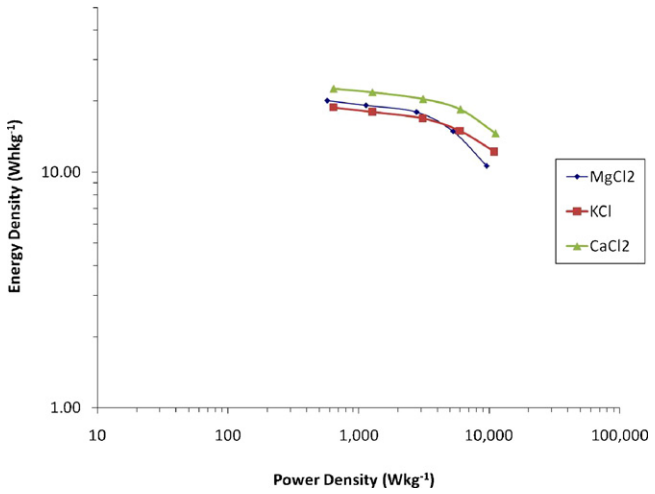

Fig. 9. Ragone plot showing the performance of asymmetric capacitors in three different electrolytes.

$$P = I\,\Delta V \tag{7}$$

where C is the cell capacitance in $F\,g^{-1}$; ΔV is the actual cell voltage (V) that accounts for instantaneous ohmic drop during both charging and discharging; I is the load current density in $A\,g^{-1}$. Ragone plots for the three systems are shown in Fig. 9.

Energy densities stored in the three capacitors were in the order $CaCl_2 > MgCl_2 > KCl$ and was 22.5, 20 and 18 Wh kg^{-1}, respectively at a power density of 1 kW kg^{-1}, which is comparable to the literature values [5,6]. In the case of $CaCl_2$ system, the capacitor was able to store almost 14 Wh kg^{-1} of energy that could be charged and discharged at 11 kW kg^{-1}.

4. Discussion

Coal tar pitch is a graphitizing precursor and, hence upon pyrolysis, it has very little porosity. Physical-chemical activation by CO_2 of the native carbon formed from CTP pyrolyisis results in only a slight increase in porosity and surface area. High surface areas are usually a property of highly disordered and non-crystalline (globally amorphous) carbons [32,33]. However, pyrolysis of coal tar pitch leads to formation of highly ordered mesophases making it difficult to create porosity. In this investigation, we sought to change the character of carbon derived from coal tar pitch so that disorder, rather than order, would be created during pyrolysis to form nanoporous carbon. Coal tar pitch is a mixture of aromatic hydrocarbons, heterocyclics and lighter, volatile organic fractions. The THF soluble fraction of the CTP has higher hydrogen content and many polycyclic heteroaromatic compounds. Many of these have been shown to be methyl derivatives which take up more space and pack less tightly when compared to the unmethylated species [34–36]. The addition of H_2SO_4 to the soluble fraction induced significant porosity in the pyrolyzed carbons. The sulfuric acid acts as oxidizing agent removing carbon and hydrogen while also incorporating oxygen functional groups in the pitch. The oxidation followed by thermal treatment facilitates polymerization and polycondensation reactions, which convert lighter volatile fractions in the pitch to heavier fractions and increase the amount of quinoline insoluble (QI) content. Petrova et al. [37,38] showed that addition of a small amount (56 mmol) of H_2SO_4 to pitch could lead to a significant increase in QI (17 wt%) and toluene insoluble 45 wt%) fractions. The increase in the QI content of the pitch also inhibits the coalescence of mesophases and increases disorder in the carbon [39]. Thus, the resultant pyrolyzed carbon showed significant nanoporosity. Carbonized QI particles could also act as highly reactive sites during CO_2 activation, thereby enhancing the apparent surface areas and pore volumes in these carbons [40]. We saw this effect during CO_2 activation and surface areas in the order of 1500–2000 $m^2\,g^{-1}$ with high yield and narrow pore size distribution (<1 nm) were developed. The presence of such small nanopores in the carbon aids strong electroadsorption of protons leading to significant shift (~−1.0 V vs. Ag/AgCl) in hydrogen evolution potential in neutral electrolytes [13–17]. The reaction at the cathode is as follows [41]:

$$C + H_2O + e^- \rightleftharpoons CH_{ads} + OH^-$$

Manganese dioxide is a low cost redox electrode that has high specific capacitance in aqueous electrolyte system. Since the pseudocapacitance is directly proportional to redox active surface area, it is important to make metal oxide particles that have both intrinsic and extrinsic surface area. Recently, Subramanian et al. have reported a facile synthesis of manganese dioxide powders with surface area as high as 250 $m^2\,g^{-1}$ and specific capacitance of 200 $F\,g^{-1}$ by a simple precipitation reaction of $KMnO_4$ with alcohol [26]. The presence of a surfactant, such as Triton-X 100, increased the microstructural control of the precipitation process, due to the formation of micelles, and made the construction of an asymmetric capacitor operable at very high power densities (11 kW kg^{-1}) possible. The formation of manganese dioxide is as follows:

$$2KMnO_4 + CH_3OH \rightarrow 2HCOOK + 2MnO_2 + H_2O$$

The pseudocapacitive nature of MnO_2 has been attributed to two possible electrochemical reactions:

$$MnO_2 + H^+ + e^- \rightleftharpoons MnOOH$$

$$MnO_2 + C^+ + e^- \rightleftharpoons MnOOC$$

The sensitivity of the specific capacitance to the pH of the electrolyte illustrates the interaction of protons with the MnO_2, while Xu et al. recently showed that manganese undergoes a change in oxidation state from Mn^{4+} to Mn^{3+} and vice versa during cycling to accommodate the intercalated cations. The size effect of the solvated cation on specific capacitance of MnO_2 was also demonstrated by Xu et al., who showed 310 $F\,g^{-1}$ in the presence of bivalent calcium cations [5]. Our studies further confirm this effect indicating that the specific capacitance could almost be doubled depending upon the type of cation used as shown in Table 1.

5. Conclusion

The paper describes a cost effective method of fabricating high energy density aqueous capacitors, from low cost precursors. Coal tar pitch was used as the low cost precursor to make high surface area carbon with controlled pore size distribution while $KMnO_4$ was used as the precursor to make high surface area redox active MnO_2. The nature of the cation strongly influenced the charge storage capacity of the electrodes with specific capacitance of manganese dioxide almost doubling in aqueous $MgCl_2$ as compared to aqueous KCl. The highest energy density was obtained in the aqueous $CaCl_2$ electrolyte system.

Acknowledgements

The authors acknowledge Consortium of Premium Carbon Products from Coal (CPCPC) for providing the funding for this project (Subcontract no: 3556-TPSU-DOE-1874) and Materials Research Institute at The Pennsylvania State University for providing access to characterization facilities.

References

[1] L.S. Zhang, International Journal of Hydrogen Energy 34 (2009) 4889–4899.
[2] P. Simon, A.F. Burke, The Electrochemical Society Interface 17 (2008) 38–43.
[3] K. Naoi, M. Morita, The Electrochemical Society Interface 17 (2008) 44–48.
[4] D. Bélanger, T. Brousse, J.W. Long, The Electrochemical Society Interface 17 (2008) 53–57.
[5] C.J. Xu, H.D. Du, B.H. Li, F.Y. Kang, Y.Q. Zeng, Journal of the Electrochemical Society 156 (2009) A435–A441.
[6] C.J. Xu, H.D. Du, B.H. Li, F.Y. Kang, Y.Q. Zeng, Journal of the Electrochemical Society 156 (2009) A73–A78.
[7] V. Khomenko, E. Raymundo-Pinero, E. Frackowiak, F. Beguin, Applied Physics A – Materials Science and Processing 82 (2006) 567–573.
[8] M.S. Hong, S.H. Lee, S.W. Kim, Electrochemical and Solid State Letters 5 (2002) A227–A230.
[9] T. Bordjiba, D. Belanger, Electrochimica Acta 55 (2010) 3428–3433.
[10] W. Chen, Z.L. Fan, L. Gu, X.H. Bao, C.L. Wang, Chemical Communications 46 (2010) 3905–3907.
[11] S.B. Ma, K.W. Nam, W.S. Yoon, X.Q. Yang, K.Y. Ahn, K.H. Oh, K.B. Kim, Journal of Power Sources 178 (2008) 483–489.
[12] S. Devaraj, N. Munichandraiah, Electrochemical and Solid State Letters (2005) A373–A377.
[13] F. Beguin, Journal of the Brazilian Chemical Society (2006) 1083–1089.
[14] F. Beguin, M. Friebe, K. Jurewicz, C. Vix-Guterl, J. Dentzer, E. Frackowiak, Carbon (2006) 2392–2398.
[15] F. Beguin, K. Kierzek, M. Friebe, A. Jankowska, J. Machnikowski, K. Jurewicz, E. Frackowiak, Electrochimica Acta 51 (2006) 2161–2167.
[16] K. Jurewicz, E. Frackowiak, F. Beguin, Fuel Processing Technology 77 (2002) 415–421.
[17] K. Jurewicz, E. Frackowiak, F. Beguin, Applied Physics A – Materials Science and Processing 78 (2004) 981–987.
[18] J.A. Macia-Agullo, B.C. Moore, D. Cazorla-Amoros, A. Linares-Solano, Carbon 42 (2004) 1367–1370.
[19] H. Teng, T.-C. Weng, Microporous and Mesoporous Materials 50 (2001) 53–60.
[20] E. Daguerre, A. Guillot, F. Stoeckli, Carbon 39 (2001) 1279–1285.
[21] K. Kierzek, E. Frackowiak, G. Lota, G. Gryglewicz, J. Machnikowski, Electrochimica Acta 49 (2004) 515–523.
[22] S. Mitani, S.-I. Lee, S.-H. Yoon, Y. Korai, I. Mochida, Journal of Power Sources 133 (2004) 298–301.
[23] A. Alonso, V. Ruiz, C. Blanco, R. Santamaria, M. Granda, R. Menendez, S.G.E. de Jager, Carbon 44 (2006) 441–446.
[24] C.L. Burket, R. Rajagopalan, H.C. Foley, Carbon 45 (2007) 2307–2310.
[25] C.L. Burket, R. Rajagopalan, H.C. Foley, Carbon 46 (2008) 501–510.
[26] V. Subramanian, H.W. Zhu, B.Q. Wei, Chemical Physics Letters 453 (2008) 242–249.
[27] R.K. Mariwala, H.C. Foley, Industrial and Engineering Chemistry Research 33 (1994) 2314.
[28] M. Chigane, M. Ishikawa, Journal of Electrochemical Society 147 (2000) 2246–2251.
[29] M. Toupin, T. Brousse, D. Belanger, Chemistry of Materials 16 (2004) 3184–3190.
[30] M. Toupin, T. Brousse, D. Belanger, Chemistry of Materials 14 (2002) 3946–3952.
[31] J.P. Zheng, Journal of Electrochemical Society 150 (2003) A484–A492.
[32] M. Acharya, M.S. Strano, J.P. Mathews, S.J. Billinge, V. Petkov, S. Shekhar, Philosophical Magazine B: Physics of Condensed Matter: Statistical Mechanics, Electronics, Optical and Magnetic Properties 79 (1999) 1499–1518.
[33] M.A. Smith, H.C. Foley, R.F. Lobo, Carbon 42 (2004) 2041–2048.
[34] M.D. Guillen, M.J. Iglesias, A. Dominguez, C.G. Blanco, Energy and Fuels 6 (1992) 518–525.
[35] M.D. Guillen, J. Blanco, J.S. Cange, C.G. Blanco, Energy and Fuels 5 (1991) 188–192.
[36] C.G. Blanco, M.D. Guillen, Industrial and Engineering Chemistry Research 30 (1991) 1579–1582.
[37] B. Petrova, T. Budinova, E. Ekinci, N. Petrov, F. Yardim, Carbon 45 (2007) 704–709.
[38] B. Petrova, T. Budinova, N. Petrov, F. Yardim, E. Ekinci, M. Razvigorova, Carbon 43 (2005) 261–267.
[39] E. Mora, R. Santamaria, C. Blanco, M. Granda, R. Menendez, Journal of Analytical and Applied Pyrolysis 68–69 (2003) 409–424.
[40] M. Granda, E. Casal, J. Bermejo, R. Menendez, Carbon 38 (2000) 2151–2160.
[41] E. Frackowiak, Journal of Physics and Chemistry of Solids 71 (2010) 692–695.